Int. J. Plant Bas. Pharm. (2023) 3(1), 104-113

INTERNATIONAL JOURNAL OF PLANT BASED PHARMACEUTICALS

https://ijpbp.com

RESEARCH ARTICLE

OPEN ACCESS

FTIR spectral correlation with alpha-glucosidase inhibitory activities of selected leafy plants extracts

Savani Ulpathakumbura[a,b], Nazrim Marikkar[a*], Lalith Jayasinghe[a]

[a] *National Institute of Fundamental Studies, Hanthana Road, Kandy, Sri Lanka*
[b] *University of Peradeniya, Postgraduate Institute of Science, Kandy, Sri Lanka*

ARTICLE INFO

Article History:

Received: 13 February 2023
Revised: 20 April 2023
Accepted: 24 April 2023
Available online: 26 April 2023

Edited by: B. Tepe

Keywords:

Leafy plants
FTIR
PLS regression analysis
Alpha-glucosidase inhibitory activity

ABSTRACT

Fourier transform infrared spectroscopy (FTIR) is a simple, rapid analytical technique used for the identification of organic functional groups of biomolecules. This study aimed to investigate the use of FTIR spectroscopy method for rapid detection of the α-glucosidase inhibitory activity of crude extracts of edible leafy plants, characterization of functional groups of chemical components present in crude extracts, and identification of possible biomolecules responsible for α-glucosidase inhibitory activity. Powdered leaves of five different plants, namely *Le-kola pala* (LE) (*Premna procumbens*), *Kora kaha* (KK) (*Memecylon umbellatum*), *Koppa* (KO) (*Polyscias scutellaria*), *Stevia* (ST) (*Stevia rebaudiana*), and *Yaki naran* (YK) (*Atlantia ceylanica*) were sequentially extracted with hexane, ethyl acetate (EtOAc) and methanol (MeOH). The FTIR spectra of crude plant extracts were obtained following the KBr pellet method, within the range of 4000-500 cm^{-1}. The plant extracts were subjected to assay the α-glucosidase inhibitory activity. Further, the multivariate predictive models for α-glucosidase inhibitory activity were developed using partial least square (PLS) regression analysis. The highest Rc^2 (0.96), Rcv^2 (0.87), Rp^2 (0.93), and the lowest RMSEC (24.10), RMSECV (41.70), and RMSEP (81.04) values were noticed for spectral region range from 1700 cm^{-1} to 1800 cm^{-1}, indicating the strongest correlation to the α-glucosidase inhibitory activity, while the spectral region range from 1500 cm^{-1} to 1700 cm^{-1} was found to have the lowest Rc^2 (0.71), Rcv^2 (0.52), Rp^2 (0.45) and the highest RMSEC (61.14) and RMSECV (80.21), indicating the lowest correlation to the α-glucosidase inhibitory activity. As the peak appearing in the range of 1700-1800 cm^{-1} is usually ascribed to C=O stretching vibration of ester groups, ketones, and carboxylic acids, there was a strong correlation between α-glucosidase inhibitory activity with those organic functional groups. The present study suggests that FTIR spectral analysis together with PLS regression analysis would be a convenient, rapid tool to determine α-glucosidase inhibitory activity of plant extracts.

1. Introduction

Diabetes Mellitus (DM) is a complex metabolic disorder occurring due to malfunctions in insulin secretion, insulin action, or both. Nowadays, it has become a serious health issue as well as a socioeconomic burden for several countries. Control of hyperglycemia is an important step as diabetes management because if left unchecked it can increase the risk of many macrovascular and microvascular complications such as hypertension, coronary vascular disease, cardiomyopathy, stroke and retinopathy, nephropathy, and neuropathy (Jayaraj et al., 2013). Recent reports pointed out that a high postprandial plasma glucose level could be more deleterious than fasting blood glucose as it can cause serious complications and increase the mortality rate. Hence, patients suffering from diabetes should need to take every possible control measures to minimize their postprandial blood glucose level (Xiao-Ping et al., 2010). One of the effective therapeutic approaches for treating diabetes is to lower the postprandial hyperglycemia level by suppressing glucose absorption through inhibition of the carbohydrate-

Reviewed by:
Walid Elfalleh: Higher Institute of Applied Sciences and Technology of Gabes, Gabes, Tunisia
Mehmet Sabih OZER: Manisa Celal Bayar University, Manisa, Türkiye

* Corresponding author(s):
E-mail address:
nazrim.ma@nifs.ac.lk (N. Marikkar)
e-ISSN: 2791-7509
doi: https://doi.org/10.29228/ijpbp.22

hydrolyzing enzymes, namely α-amylase and α-glucosidase (De Souza Schmidt Goncalves et al., 2010; Nickavar & Abolhasani, 2013). According to Western medical practice, acarbose can help in blunting the postprandial plasma glucose rise by prolonging the enzymatic hydrolysis of complex carbohydrates, thereby delaying glucose absorption (Shobana et al., 2009). To date, some α-amylase and α-glucosidase inhibitors have been isolated from medicinal plants to serve as an orthodox drugs with increased potency and mild side effects when compared to existing synthetic drugs (Kazeem et al., 2013).

For decades, the consumption of several types of leafy plants is advocated for the control and management of postprandial blood glucose. According to a compilation by Ediriweera and Ratnasooriya (2009), edible leafy plants, such as *Kiri anguna* (*Tylophora pauciflora*), *Thebu* (*Costus speciosus*), *Curry plant* (*Murraya koenigii*), *Kowakka* (*Coccinia grandis*), *Adhathoda* (*Adhathoda vasica*), *Mukunuwenna* (*Alternanthera sessilis*), *Ranawara* (*Cassia auriculata*), *Gotukola* (*Cantella asiatica*) are already recognized as effective in controlling diabetes. Aside from these, there are some lesser-known leafy plants, namely *Le-kola pala* (*Premna procumbens*), *Koppa* (*Polyscias scutellaria*), *Stevia* (*Stevia rebaudiana*), *Yaki naran* (*Atlantia ceylanica*), and *Kora kaha* (*Memecylon umbellatum*) which are also believed to have anti-diabetic effect according to traditional knowledge. However, studies are needed to confirm that their anti-diabetic potential is little or insufficient. Currently, various in vitro and in vivo assays are employed in exploratory studies to establish their effectiveness for diabetes. In vitro studies usually adopt parameters that include enzymatic assays related to glucose metabolism while in vivo studies investigate the analysis of anti-diabetic efficacy by biochemical parameters such as blood glucose, insulin, and serum protein (Bhardwaj et al., 2020). The established in vitro methods are, however, rather lengthy, labor-intensive, and require several chemical reagents. Owing to these reasons, there has been a continuous urge in the scientific community to find out simple, cost-effective, and rapid methods to detect α-glucosidase inhibitory activity of emerging foods or plant-based products.

In recent times, FTIR spectroscopy has emerged as a rapid analytical tool for chemical mapping of natural plant extracts and various other products (Gunarathne et al., 2022b). Although this technique was used in the early days for the identification of functional groups in organic molecules, its application range has now broadened to include complex issues related to chemical and biological systems. In food industries, FTIR spectroscopy has been widely investigated for authentication and quality control of food and drugs (Gunarathne et al., 2022a), determination of enzyme activity of sea buckthorn substrate (Adina et al., 2010), and efficacy of herbal medicinal formulations (Ashokkumar & Ramaswamy, 2014; Bunaciu et al., 2011). In comparison to chromatographic techniques, FTIR has become popular due to its rapidity and ease of operation. As it could be applied together with multivariate data analysis, FTIR could help generate predictive models useful for chemical analysis (Easmin et al., 2017). According to some reports, FTIR spectral data combined with multivariate data analysis have been successful to develop predictive models for α-glucosidase inhibitory activity of novel plant extracts (Easmin et al., 2017; Saleh et al., 2018; Umar et al., 2021). The objective of this study was to assess FTIR spectral correlation with α-glucosidase inhibitory activities of selected anti-diabetic leafy plants, namely *Le-kola pala* (LE) (*P. procumbens*), *Koppa* (KO) (*P. scutellaria*), *Stevia* (ST) (*S. rebaudiana*), *Yaki naran* (YK) (*Atlantia ceylanica*), and *Kora kaha* (KK) (*M. umbellatum*). The outcomes of this study would be useful to establish a database of local plant species, which demonstrate moderate to high anti-hyperglycaemic effects.

2. Materials and methods

2.1. Plant materials

Five edible leafy plants, namely *Le-kola pala* (LE) (SULE21004), *Kora kaha* (KK) (SUKK21003), *Koppa* (KO) (SUKO21002), *Stevia* (ST) (SUST21001), and *Yaki naran* (YK) (SUYK21005) were used in this study. Samples were collected from the Central and North Central Provinces of Sri Lanka from March 2021 to May 2021. The plants were cross-checked by Dr. D. S. A. Wijesundera, Senior Taxonomist from the Royal Botanical Garden of Sri Lanka, and their voucher specimens were deposited in Popham's Arboretum of NIFS in Dambulla, Sri Lanka. The collected samples were cleaned under running tap water and dried at 55 °C for 8-10 hours in a forced-convection air-drying oven (Biobase, model-BOV-V230F, China). The dried leaves were ground into powder and stored at 4 °C for further analysis.

2.2. Preparation of crude extracts

Two hundred grams of powdered leaves of each plant species were sequentially extracted with hexane, EtOAc, and MeOH using ultra-sonication (Rocker ultrasonic cleaner, model-Soner 206H) for 30 min. For each solvent type, the extraction was repeated three times. Each plant extract type was concentrated using a rotary evaporator (Heidolph, Laborota 4000) under reduced pressure followed by vacuum drying (vacuum oven, Heraeus instrument, Germany) for 3-4 hours. The crude extracts were stored at -18 °C for further analysis.

2.3. Determination of α-glucosidase inhibitory activity

α-Glucosidase inhibitory activity of crude plant extracts was determined according to the method described by Gunarathne et al. (2022c). Briefly, a concentration series (3.91-1000 ppm) of plant extracts were prepared by dissolving the crude extracts in distilled water with 3% DMSO. Thereafter, 100 µl of 30 mM phosphate buffer (pH 6.5) was added into 96 wells micro-plate, followed by mixing with 25 µl of sample solution (reconstituted crude extract with distilled water). In the next step, 25 µl α-glucosidase enzyme solution (12.5 µl/ml) was added to it and incubated for 5 min at 37 °C. After that, a 50 µl portion of pNPG (*p*-nitrophenyl-α-D-glucopyranoside) solution (0.8 mg/ml) was added and followed by incubation for another 30 min at 37 °C. In the present study, acarbose (Glucobay tablet) was used as the positive control. The absorbance value was measured at 410 nm and the percentage of α-glucosidase inhibitory activity was calculated using the following equation. The IC_{50} values were calculated graphically by plotting the percentage of α-glucosidase inhibition against the sample concentration of each extract.

$$Percentage\ \alpha - glucosidase\ inhibition = \frac{\delta A_{control} - \delta A_{sample}}{\delta A_{control}} x\ 100 \quad \ldots\ldots(1)$$

where;

$\delta A_{control}$ = $Absorbance_{control}$ - $Absorbance_{control\ blank}$

δA_{sample} = $Absorbance_{sample}$ - $Absorbance_{sample\ blank}$

2.4. FTIR measurements

FTIR analysis of crude extracts was performed according to the KBr pellet method as described by Mittal et al. (2020) and Gunarathne et al. (2022b) with some modifications. Initially, approximately 1 mg of each crude extract was mixed with 100 mg of KBr (FT-IR grade, ≥ 99% trace metals basis, Sigma Aldrich) and made into a pellet using a hydraulic press. The spectra were recorded using an FTIR Nicolet iS50 spectrometer (Thermo Nicolet, Madison, WI) equipped with deuterated triglycine sulfate (DTGS) KBr detector and KBr beam splitter. The data were obtained in the mid-infrared region of 4000-500 cm^{-1} by co-adding at 64 scans with resolution, resolution of 8 cm^{-1}. All spectra were ratioed against a background spectrum of pure KBr pallet. The absorbance values were recorded at each data point in triplicate.

2.5. Statistical analysis

α-Glucosidase inhibitory measurements were obtained at least in triplicate data (n=3) and the results were presented as mean ± standard deviation (SD). Data were analyzed statistically by one-way ANOVA using Minitab 17 software package. When the F values were significant, mean differences were compared using Tukey's test at the 5% level of probability.

2.6. Spectral analysis

The manufacturer's software (OMNIC operating system, version 7.0 Thermo Nicolet) was used for spectral pre-processing and qualitative analysis. The raw spectra of each plant extract were subjected to baseline correction and scale normalization, respectively. The mean spectrum of the triplicates was used for qualitative purposes.

2.7. PLS regression analysis

The Unscrambler 9.7 (Camo, USA) software was used to perform the PLS regression analysis for spectral data of crude extracts as described by Gunarathne et al. (2022a). Initially, four replicates of 14 crude extracts were collected and followed by randomly dividing into two sets (i.e., 38 elements to use for calibration and cross-validation and 18 elements to test the predictive models). The predictive models were developed by using the total spectra range (3700-500 cm^{-1}) and different spectra ranges (A: 3700-2800 cm^{-1}; B: 1800-1700 cm^{-1}; C: 1700-1500 cm^{-1}; D: 1500-900 cm^{-1}: E: 900-500 cm^{-1}). The best predictive model for α-glucosidase inhibitory activity was identified by comparing the model parameters including, coefficient of determination of calibration (Rc^2), root mean square errors of calibration (RMSEC), coefficient of determination of prediction (Rp^2), root mean square errors of prediction (RMSEP), coefficient of determination of cross-validation (Rcv^2), root mean square errors of cross-validation (RMSECV).

3. Results and discussion

The spectral overlays given in Figures 1(A), (B), and (C) represent the characteristic bands of the plant extracts obtained from hexane, EtOAc, and MeOH, respectively. The aim of interpreting them was to characterize the organic functional groups as parameters for monitoring α-glucosidase inhibitory activity exhibited by the plants of this study. Assignments of spectral bands falling into different regions of the spectrum (A: 3700-2800 cm^{-1}; B: 1800-1700 cm^{-1}; C: 1700-1500 cm^{-1}; D: 1500-900 cm^{-1}: E: 900-500 cm^{-1}) were made to different organic functional groups based on previous reports listed in Tables 1 and 2.

3.1. Characterization of region A in 3700-2800 cm^{-1}

According to the overview shown in Figure 1(A), the spectral patterns of hexane extracts of the plants differed only slightly in different regions. Broad absorption peaks in the region 3500-3400 cm^{-1} were displayed by all plant extracts. According to Table 1, the broad blunt peak H1 centered at ~3440 cm^{-1} represents the O–H stretching vibration of phenols, alcohols, complex carbohydrates, etc. (Coates, 2000; Nandiyanto et al., 2019). The highest intensity was shown by KO while the lowest intensity was displayed by LE. The high intensity of the H1 peak confirmed the abundance of complex carbohydrates in the hexane extract of KO. On the other hand, the H1 peak appearing as a low-height peak in the hexane extract of LE would indicate a relatively lower amount of the above-mentioned molecules in LE. According to the spectral overlay of EtOAc extracts, as shown in Figure 1(B), the broad blunt peaks (E1) were now centered at ~3400 cm^{-1}, indicating a slight shift in frequency. All EtOAc extracts exhibited an enhancement in the peak intensity when compared to those of hexane extracts. Both KO and ST gave high intensity while others showed low intensity. As mentioned previously in the hexane extract of LE, the broad and low height peak (E1) appearing at 3400 cm^{-1} indicated comparatively lower amount of phenols, alcohols, and carbohydrates in the EtOAc extract of LE. The same was true for the EtOAc extract of KK. Nevertheless, the intensity of peak E1 of KO appearing at ~3400 cm^{-1} was slightly higher than that of peak H1 of KO, indicating the relatively higher abundance of phenols, alcohols, and carbohydrates in EtOAc extracts. The spectral overlay of MeOH extracts in Figure 1(C) shows that all plants exhibited the highest peak intensity for the broad blunt peak (M1), which was centered at ~3410 cm^{-1}. There was a huge enhancement effect on this peak (M1) when compared to those of either hexane or EtOAc extracts. This could be probably due to the fact that the concentration of carbohydrates, phenolics or aliphatic alcohols, etc. would have become high in MeOH extracts due to the effect of sequential extraction.

In the majority of the plant extracts, aliphatic chains occur as components of various biomolecules including lipids, carotenoids, etc. The occurrence of some amount of *cis* and *trans* double bonds as a part of alkenes is common in many cases. The spectral overlay of both hexane and EtOAc extracts as illustrated in Figures 1(A) and (B) gave evidence for the presence of a weak band corresponding to terminal (vinyl) C–H stretching vibration of alkenes. In Figure 1(B), peak E2 appearing at ~3010 cm^{-1} is usually ascribed to terminal (vinyl) C–H stretching of alkenes. Therefore, the high-intense E2 peak in the EtOAc extract of ST could be due to the high-presence of alkenes. According to the spectral overlay of MeOH extracts, as given in Figure 1(C), this weak band was masked due to overlapping caused by the broad blunt peaks (M1) which were centered at ~3410 cm^{-1}. It could also be noted that the influence of lipids with some degrees of unsaturation could be present more in both hexane and EtOAc extracts when compared to MeOH extracts.

The prominent H3 (at ~2925 cm^{-1}) and H4 (~2854 cm^{-1}) peaks in hexane extracts as shown in Figure 1(A) was due to the asymmetrical and symmetrical C–H stretching of methylene groups, respectively (Coates, 2000; Nandiyanto et al., 2019). According to previous studies, these two were quite commonly encountered in the spectra of major edible plant oils and animal fats (Gunarathne et al., 2022b). Among hexane extracts, ST was found to display high-intensity peaks for H3. Meanwhile, among hexane extracts, KK displayed a comparatively high-intense peak for H4. According to spectral overlay as illustrated in Figure 1(B), E3 and E4 peaks of EtOAc extracts were also assigned to the same spectral vibrations.

The prominence of these two peaks was probably due to the heavy presence of aliphatic chains attached to lipids, carotenoids, carbohydrates, and other ester compounds (Table 1). When considering the spectral intensities, the EtOAc extract of LE was found to exert relatively high intensity for peaks E4. As mentioned earlier, E4 confirmed the higher existence of CH_2 groups in the EtOAc extract of LE. A closer look at the spectral patterns illustrated in Figures 1(A) and (B) would suggest that the intensities of these two peaks of hexane extracts were a little higher than those of these two peaks in EtOAc extracts. According to spectral overlay as illustrated in Figure 1(C), the intensities of these two peaks sharply declined in all MeOH extracts. With the prominence of the broad blunt peak (M1) of MeOH extracts centered at ~3410 cm^{-1}, a decline in the intensities of M3 and M4 peaks was noticable. This could be partly due to decreases in the proportion of molecules with aliphatic chains in MeOH extracts after sequential extraction. According to previous studies, extraction with hexane and EtOAc could usually take away most of the lipid biomolecules (Gunarathne et al., 2022b). Among all MeOH extracts, intensities of M3 and M4 peaks of ST and KO were slightly higher than those of the rest of the plant extracts.

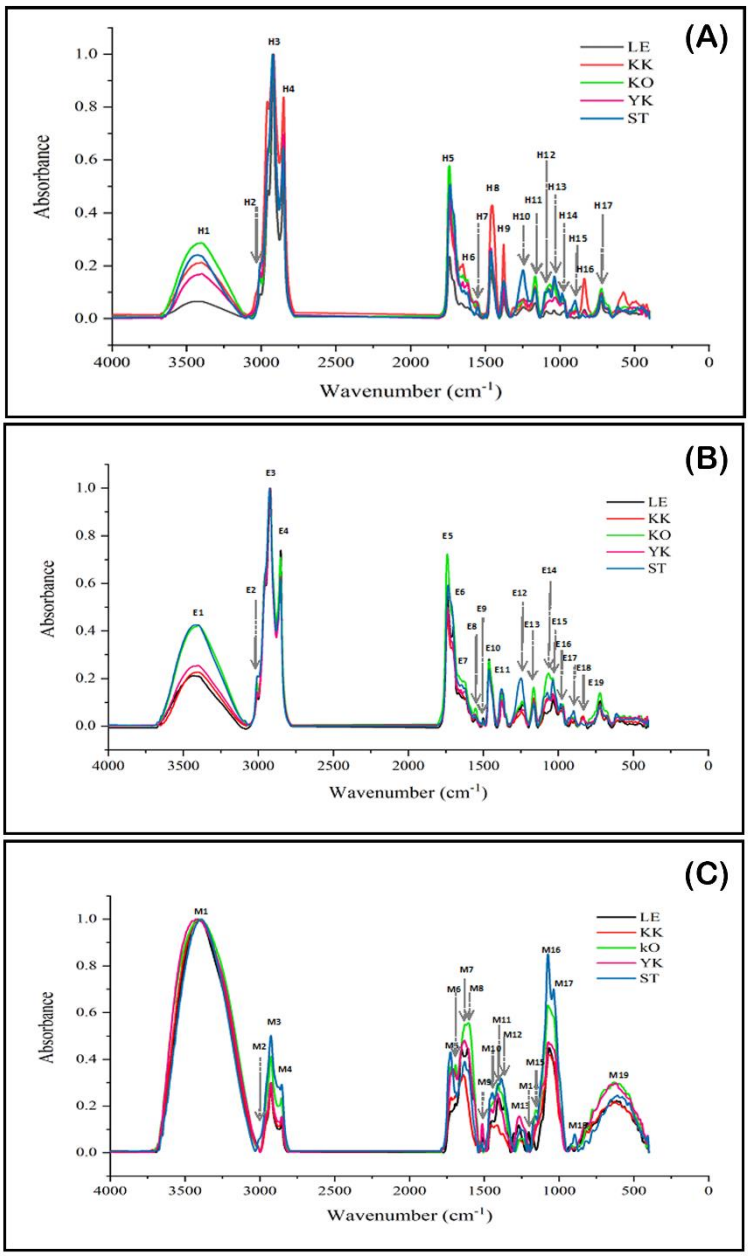

Figure 1. FTIR spectral overlay of hexane (A), ethyl acetate (B) and methanol (C) extracts of leafy plants

3.2. Characterization of region B in 1800-1700 cm^{-1}

The ester groups were always part of various biomolecules present in both hexane and EtOAc extracts. For instance, the majority of oils, fats, waxes, etc. are used to exhibit C=O stretching vibration due to ester groups present in acylglycerol molecules (Coates, 2000; Nandiyanto et al., 2019). According to the spectral overlays in Figures 1(A) and (B), in most of the plant extracts, there appeared the characteristic sharp peaks H5 and E5 centered at ~1742 cm^{-1}. Among hexane extracts, KO showed a high-intense for H5 peak while LE showed a low-intense peak at ~1742 cm^{-1} (H5). Among EtOAc extracts, the high-intense E5 peak denoted the comparatively higher existence of compounds with ester linkage and alkyl carbonates (Figure 1B). This difference could be probably due to the

relative differences in the abundance of compounds with ester linkage in these two types of extracts. According to Figure 1(C), peak M5 at 1730 cm^{-1} was present in all MeOH extracts, but their peak intensities were comparably lower than those of both hexane and EtOAc extracts. This observation suggests that a decrease happened in the proportion of molecules bearing ester functional groups in MeOH extracts with the sequential extraction. By contrast to hexane extracts, EtOAc extracts were found to have an additional peak E6 at ~1706-1712 cm^{-1}. Based on Table 1, this could be assigned to C=O stretching vibration associated with either carboxylic acids or ketones. For instance, a moderate-intense peak of E6 represented the moderate existence of carboxylic acids/ketones in the EtOAc extract of LE. The same is true for MeOH extracts, which also exhibited a peak (M6) at ~1706 cm^{-1} which would indicate the presence of C=O stretching vibration of either carboxylic acids or ketones. However, any peak in this wavenumber range (~1706 cm^{-1}) was not exhibited by the MeOH extract of ST. According to Figure 1(C), this peak in MeOH extracts is represented by M6 which appeared as a high-intense peak for both KO and YK.

Table 1. Characterization of FTIR spectra of hexane and EtOAc extracts of leafy plants

Peak no	Wavenumber range* (cm^{-1})	Mode of vibration	Functional group	Reference
H1, E1	3400-3440	O–H stretching	Carbohydrates/Phenols/Alcohols	(Coates, 2000; Nandiyanto et al., 2019)
H2, E2	3010-3013	Terminal (vinyl) C–H stretching	Alkenes	(Coates, 2000; Nandiyanto et al., 2019)
H3, E3	2925-2928	Methylene C–H asymmetric stretching	(CH_2) Alkanes	(Coates, 2000; Nandiyanto et al., 2019)
H4, E4	2852-2857	Methylene C–H symmetric stretching	(CH_2) Alkanes	(Coates, 2000; Nandiyanto et al., 2019)
H5, E5	1739-1745	C=O stretching	Ester groups/Alkyl carbonates	(Coates, 2000; Nandiyanto et al., 2019)
E6	1706-1712	C=O stretching	Carboxylic acids/Ketones	(Coates, 2000; Nandiyanto et al., 2019)
H6, E7	1630-1658	C=O stretching	Amides	(Coates, 2000; Nandiyanto et al., 2019; Nokhala et al., 2020)
		C=C skeletal stretching	Alkene	
		N-H bending	Primary/Secondary amines	
		–C=N– stretching	Imines	
		–N=N– stretching	Azo compounds	
H7, E8	1550-1565	> N–H bending	Secondary amines	(Coates, 2000; Nandiyanto et al., 2019; Nokhala et al., 2020)
		N=O asymmetric stretching	Aliphatic nitro compounds	
E9	1503-1506	C=C–C stretching	Aromatic rings	(Coates, 2000; Nandiyanto et al., 2019)
		NO_2 asymmetric stretching	Aromatic nitro compounds	
H8, E10	1459-1468	Methyl C–H asymmetric bending	Methyl C–H asymmetric bending-CH_3	(Coates, 2000; Nandiyanto et al., 2019)
		Methylene C–H bending	Methylene C–H bending CH_2	
H9, E11	1380-1383	N=O symmetric stretching	Aliphatic nitro compounds	(Hari & Nair, 2018; Nipun et al., 2020)
H10, E12	1247-1256	Aryl–O stretching	Aromatic ethers	(Coates, 2000; Nandiyanto et al., 2019; Saleh et al., 2018)
		C–N stretching	Aromatic primary amines	
H11, E13	1165-1171	C–N stretching	Secondary amines	(Coates, 2000; Nandiyanto et al., 2019)
H12, E14	1068-1080	C–N stretching	Primary amines	(Coates, 2000; Nandiyanto et al., 2019)
		C–O stretching	Ethers	
		C–O stretching	Cyclic ether	
H13, E15	1035-1044	C–O stretching	Primary alcohols	(Coates, 2000; Nandiyanto et al., 2019)
H14 + H15, E16 + E17	(976-988) + (900-918)	Vinyl C–H out-of-plane bending	Alkenes	(Coates, 2000; Nandiyanto et al., 2019)
H16, E18	838-841	Aromatic C–H out-of-plane bending (C–H 1,4-disubstitution-*para*)	Aromatic ring	(Coates, 2000; Nandiyanto et al., 2019)
H17, E19	723-726	Methylene-$(CH2)_n$-rocking	Hydrocarbon	(Coates, 2000; Nandiyanto et al., 2019)

*Range of variation in wavenumbers at a particular peak among the different edible leafy plants namely; *Le-kola pala, Kora kaha, Koppa, Yaki naran* and *Stevia*

3.3. Characterization of region C in 1700-1500 cm^{-1}

Distinct variations were seen in this range for different plant extracts as shown in Figures 1(A), (B) and (C). The occurrence of H6 and H7 was noticed in hexane extracts while the occurrence of E7, E8, and E9 was observed in EtOAc extracts. According to Figure 1(C), peaks M6, M7, M8, and M9 were found in this range for MeOH extracts. This indicated the effect of sequential extraction on chemical compositional changes of the plant extracts. Based on the information provided in Table 1, most of the hexane extracts were found to have the blunt peak (H6) at ~1655 cm^{-1}, which was attributed to C=O stretching of amides, C=C skeletal stretching of alkenes and C=N stretching of imines. The high-intensity peak of H6 could indicate the relatively high presence of amides and alkenes in the hexane extract of KK. The blunt peak E7 of EtOAc extracts appearing in the range of 1630-1633 cm^{-1} is usually assigned for C=O stretching of amides, C=C skeletal stretching of alkenes, N–H bending of primary and secondary amines, –C=N– stretching of open chain imines and –N=N– stretching of open chain azo compounds (Coates, 2000; Nandiyanto et al., 2019; Nokhala et al., 2020). Among EtOAc extracts, KO exhibited the high-intense peak of E7, indicating the high existence of amides, alkenes, primary amines/secondary amines, imines, and azo compounds. As shown in Figure 1(C), the peak M7 appeared within the range of 1633-1659 cm^{-1} is usually assigned to C=O stretching of amides, C=C skeletal stretching of alkenes, N–H bending of primary and secondary amines, –C=N– stretching of open chain imines (Coates, 2000; Nandiyanto et al., 2019; Nokhala et al., 2020). Among MeOH extracts, KO exhibited the high-intense peak of M7. According to Figure 1(C), among MeOH extracts, KO showed a high-intense peak for M8. The peak M8 is ascribed to the conjugated C=C stretching vibration of alkenes, C=C–C stretching of the aromatic ring, C=O stretching of carboxylates, N–H bending of primary and secondary amines, –C=N– stretching of open chain imines and –N=N– stretching of open chain azo compounds, which exhibited a peak at ~1603-1615 cm^{-1} (Coates, 2000; Nandiyanto et al., 2019; Nokhala et al., 2020). However, this peak did not occur in both hexane and EtOAc extracts.

As shown in Figure 1(A), the peak H7 appearing at ~1559 cm^{-1} is attributed to > N–H bending of secondary amines and N=O stretching of aliphatic nitro compounds (Coates, 2000; Nandiyanto et al., 2019; Nokhala et al., 2020). As illustrated in Figure 1(B), the peak E8 of EtOAc extracts, observed at ~1550 cm^{-1} indicated the presence of > N–H bending of secondary amines and N=O asymmetric stretching of aliphatic nitro compounds (Coates, 2000; Nandiyanto et al., 2019; Nokhala et al., 2020). Among EtOAc extracts, the highest intensity for E8 was displayed by KO, but none

of the crude extracts of MeOH was found to show a peak in the range of 1559-1550 cm^{-1}.

According to Table 1, the peak E9 (~1503 cm^{-1}) is usually ascribed to C=C–C stretching vibration and NO_2 asymmetric stretching vibration of aromatic rings and aromatic nitro compounds, respectively (Coates, 2000). Among EtOAc extracts, this peak appeared as a minute peak, indicating a relatively lower existence of aromatic rings and aromatic nitro compounds in EtOAc extracts. In the case of the MeOH extract of YK, a high-intensity peak was observed for M9. As the peak M9, appearing at ~1515 cm^{-1} would result due to C=C–C stretching of aromatic rings and NO_2 asymmetric stretching of aromatic nitro compounds, the high-intensity peak of M9 would indicate the higher existence of aromatic rings and aromatic nitro compounds in YK (Coates, 2000; Nandiyanto et al., 2019).

3.4. Characterization of region D in 1500-900 cm^{-1}

This particular region of the spectra (1500 cm^{-1}-900 cm^{-1}) is usually known by researchers as the fingerprint region. Hence, it is the region that gives spectral features which are unique to different materials. According to Figure 1(A), the narrow sharp peak (H8) existing at ~1459 cm^{-1} denotes the asymmetric C–H bending of methyl groups and C–H bending vibration of methylene groups in aliphatic chains. Among hexane extracts, KK displayed comparatively high-intense peak for H8. Again, the narrow sharp peak E10 observed among EtOAc extracts at ~1465 cm^{-1} indicates the asymmetric C-H bending of methyl groups and C–H bending vibration of methylene groups in aliphatic chains (Figure 1B). Among the crude EtOAc extracts, LE was found to exert relatively high intens peak for E10. The forgone discussion suggested that the number of lipid biomolecules gets reduced in MeOH extracts as a result of sequential extraction with hexane and EtOAc. Hence, the peak M10 appearing at ~1450 cm^{-1} among MeOH extracts is ascribed to the C=C–C stretching of aromatic rings (Coates, 2000; Nandiyanto et al., 2019). In Figure 1(A), peak M11 existing at ~1403 cm^{-1} would result due to either vinyl C–H in-plane bending vibration of alkenes or O–H bending of phenols/tertiary alcohols. As seen from Figures 1(A) and (C), this peak did not appear to emerge in both hexane or EtOAc extracts. Among MeOH extracts, both KO and ST showed high-intense peaks for M11.

As shown in Figure 1(A), peak H9 appearing at ~1380 cm^{-1} was attributed to the N=O symmetric stretching of aliphatic nitro compounds. This was further confirmed by the presence of aliphatic nitro compounds in hexane extracts of edible leafy plants (Hari & Nair, 2018; Nipun et al., 2020). For instance, a higher abundance of aliphatic nitro compounds in the hexane extract of KO was further confirmed by the high-intense peak H9 appearing at ~1380 cm^{-1}. In the case of EtOAc extracts, peak E11 represented N=O symmetric stretching vibration of aliphatic nitro compounds, in this ST showed a highly intense peak (Figure 1B). Among MeOH extracts, the peak M12 appearing at ~1370 cm^{-1} is attributed to both methyl C–H symmetric bending vibration and N=O symmetric stretching vibration, indicating the presence of alkanes and aliphatic nitro compounds. According to Figure 1(A), peak H10 found at ~1250 cm^{-1} indicates the aryl–O stretching of ethers and C–N stretching of aromatic primary amines in plants (Coates, 2000; Saleh et al., 2018). Among hexane extracts, ST was found to display a high-intense-peak for H10. The presence of a high-intense peak for H10 indicated a higher abundance of aromatic ethers and aromatic primary amines in the hexane extract of ST (White, 1971). Among EtOAc extracts, peak E12 centered at ~1250 cm^{-1} represented the aryl–O stretching of aromatic ethers and C–N stretching of aromatic primary amines in plants (Figure 1B) (Coates, 2000; Saleh et al., 2018). Among the five plants used in this study, ST exhibited the most intense E12 peak. Among MeOH extracts, the peak M13 appearing at ~1270 cm^{-1} is usually ascribed to the aryl–O stretching of aromatic ethers and the C–N stretching of aromatic primary amines. In addition to this, the in-plane blending of O–H of primary and secondary alcohols in plants also contributes to this (Coates, 2000; Saleh et al., 2018). As shown in Figure 1(C), peak M14 existing at 1206 cm^{-1} would result due to the C–O stretching of phenols (Nandiyanto et al., 2019). Among the MeOH extracts, only LE and ST displayed peak M14 (Figure 1C). However, this peak was not seen in any of the plant extracts from hexane and EtOAc (Figure 1B).

As described in Table 1, peak H11 at ~1168 cm^{-1} is generally assigned to the C–N stretching vibration of secondary amines. When compared to other plants, KO displayed a high-intense peak for H11 (Figure 1A). The high-intense peak for H11 would indicate the higher abundance of secondary amine in the hexane extract of KO. Among EtOAc extracts, the corresponding peak representing the presence of secondary amines in all plants is peak E13 (Figure 1B). Concerning E13, KO gave the highest intense peak. Nevertheless, among MeOH extracts, peak M15 appearing within the range of 1159-1174 cm^{-1} represented the C–N stretching of secondary/tertiary amines (Coates, 2000; Nandiyanto et al., 2019). Although all MeOH extracts showed this peak, their signals appeared as a weak-shoulder peak with some overlap.

As shown in Figure 1(A), peak H12 centered within the range of 1074-1080 cm^{-1} is supposed to represent the C–N stretching of primary amines, C–O stretching of alkyl-substituted ethers, and C–O stretching of cyclic ethers. When compared to other plants, the hexane extract of KO displayed high-intense peak for H12. The high-intensity peak of H12 denoted the higher existence of primary amines, alkyl substituted ethers, and cyclic ethers in KO. As elaborated in Table 2, the peak E14 appearing at 1068 cm^{-1} is ascribed to C–N stretching of primary amines, C–O stretching of alkyl substituted ethers, and cyclic ethers (Figure 1B). The low-intense peak E14 in LE at ~1068 cm^{-1} indicated the low levels of primary amines, ethers, and cyclic ethers in LE (Coates, 2000; Nandiyanto et al., 2019). According to Figure 1(C), the peak M16 of MeOH extracts was parallel to H12 of hexane extracts and E14 of EtOAc extracts. As elaborated in Table 2, those occuring within the range of 1068-1079 cm^{-1} would represent C–N stretching of primary amines and C–O stretching of alkyl-substituted ethers and cyclic ethers (Coates, 2000; Nandiyanto et al., 2019). Among MeOH extracts, ST exhibited the high-intense peak for M16.

As illustrated in Figure 1(A), peak H13 at ~1040 cm^{-1} is usually ascribed to the C–O stretching of primary alcohols (Nandiyanto et al., 2019). Among hexane extracts, ST exhibited the high-intense peak for H13, indicating the highest abundance of molecules with primary alcohols. As shown in Figure 1(B), E15 of EtOAc within the spectral region of 1035-1041 cm^{-1} represented the C–O stretching vibration of primary alcohols. Among the plants, both KO and ST displayed the high intense peak for this. According to Figure 1(C), peak M17 of MeOH extracts was parallel to peak H13 and E15 representing the C–O stretching vibration of primary alcohols which is present at the spectral range of 1038-1041 cm^{-1} (Coates, 2000). Among the plants, ST displayed the high-intensity peak for M17 indicating a higher abundance of primary alcohols in ST.

The peaks H14 and H15 within the spectral region from 988 cm^{-1} to 900 cm^{-1} represent the vinyl C–H out-of-plane bending of alkenes (Table 1). For H14 and H15, ST displayed high-intensity peaks while

LE displayed low-intensity minute peaks (Figure 1A). This is indicative of the differences between ST and LE with regard to the abundance of vinyl C–H out-of-plane bending vibration associated with alkenes. Among EtOAc extracts, the occurrence of E16 and E17 peaks within the spectral ranges of 976-988 cm^{-1} and 900-918 cm^{-1} confirmed the existence of vinyl C–H out-of-plane bending vibrations of alkenes (Figure 1B). KK exhibited low-intensity peaks for E16 and E17, indicating the lower abundance of vinyl C–H out-of-plane bending of alkenes. However, the occurrence of the peak corresponding to vinyl C–H out-of-plane bending of alkenes was hardly detected among MeOH extracts (Figure 1C).

Table 2. Characterization of FTIR spectra of MeOH extracts of leafy plants

Peak no	Wavenumber range* (cm^{-1})	Mode of vibration	Functional group	Reference
M1	3400-3440	O–H stretching	Carbohydrates/Phenols/Alcohols	(Coates, 2000; Nandiyanto et al., 2019)
M2	3010-3013	Terminal (vinyl) C–H stretching	Alkenes	(Coates, 2000; Nandiyanto et al., 2019)
M3	2928-2931	Methylene C–H asymmetric stretching	Alkanes (CH_2)	(Coates, 2000; Nandiyanto et al., 2019)
M4	2854-2860	Methylene C–H symmetric stretching	Alkanes (CH_2)	(Coates, 2000; Nandiyanto et al., 2019)
M5	1728-1733	C=O stretching	Esters	(Coates, 2000; Nandiyanto et al., 2019)
M6	1698-1715	C=O stretching	Carboxylic acids/Ketones	(Coates, 2000; Nandiyanto et al., 2019)
M7	1633-1659	C=O stretching	Amides	(Coates, 2000; Nandiyanto et al., 2019; Nokhala et al., 2020)
		C=C skeletal stretching	Alkene	
		N–H bending	Primary/Secondary amines	
		–C=N– stretching	Imines	
M8	1603-1615	Conjugated C=C stretching	Alkenes	(Coates, 2000; Nandiyanto et al., 2019; Nokhala et al., 2020)
		C=C–C stretching	Aromatic rings	
		C=O stretching	Carboxylates	
		N–H bending	Primary/Secondary amines	
		–C=N– stretching	Imines	
		–N=N– stretching of open chain azo compounds	Azo compounds	
M9	1515-1518	C=C–C stretching asymmetric stretching of NO_2	Aromatic rings	(Coates, 2000; Nandiyanto et al., 2019; Nokhala et al., 2020)
			Aromatic nitro compounds	
M10	1450-1459	C=C–C stretching	Aromatic rings	(Coates, 2000; Nandiyanto et al., 2019; Nokhala et al., 2020)
		Methyl C–H asymmetric bending	Alkanes (CH_3)	
		Methylene C-H bending	Alkanes (CH_2)	
M11	1403-1418	Vinyl C–H in-plane-bending	Alkenes	(Coates, 2000; Nandiyanto et al., 2019; Nokhala et al., 2020)
		OH bending	Phenol/Tertiary alcohols	
M12	1370-1390	Methyl C–H symmetric bending	Alkanes (CH_3)	(Hari & Nair, 2018; Nipun et al., 2020)
		N=O symmetric stretching	Aliphatic nitro compounds	
M13	1268-1271	Aryl–O stretching	Aromatic ethers	(Coates, 2000; Nandiyanto et al., 2019; Saleh et al., 2018)
		C–N stretching	Aromatic primary amines	
		OH in-plane bending	Primary or secondary alcohol	
M14	1206	C–O stretching	Phenols	(Nandiyanto et al., 2019)
M15	1159-1174	C–N stretching	Secondary/Tertiary amines	(Coates, 2000; Nandiyanto et al., 2019)
M16	1068-1079	C–N stretching	Primary amines	(Coates, 2000; Nandiyanto et al., 2019)
		C–O stretching	Ethers	
		C–O stretching	Cyclic ethers	
M17	1038-1041	C–O stretching of primary alcohols	Primary alcohols	(Coates, 2000; Nandiyanto et al., 2019)
M18	903-925	C–C skeletal vibration	Alkanes	(Coates, 2000; Nandiyanto et al., 2019)
M19	628-630	Alkyne C–H bending	Aromatic ring	(Coates, 2000; Nandiyanto et al., 2019)
		OH out-of-plane bending	Alcohol	

*Range of variation in wavenumbers at a particular peak among the different edible leafy plants namely; *Le-kola pala, Kora kaha, Koppa, Yaki naran* and *Stevia*

3.5. Characterization of region E below 900 cm^{-1}

As shown in Figure 1(A), peak H16 appearing at ~841 cm^{-1} was due to aromatic C–H out-of-plane bending vibration. Among hexane extracts, KK displayed a relatively high-intense peak for H16, probably due to the high occurence of molecules with aromatic rings in the hexane extract. In the case of the rest of the plant extracts, only a minute peak was seen for H16, indicating the lower abundance of aromatic C–H out-of-plane bending vibration. When considering EtOAc extracts, the peak E18 appearing at ~838 cm^{-1} represented aromatic C–H out-of-plane bending vibration (Figure 1A). However, peak corresponding to aromatic C–H out-of-plane bending of aromatics was not detected among MeOH extracts. According to Figure 1(A), the distinct narrow peak H17 appearing at ~723 cm^{-1} indicated the rocking vibration of the methylene group, confirming molecules with aliphatic hydrocarbon chains in hexane extracts (Coates, 2000; Nandiyanto et al., 2019). Among the plant extracts, KO displayed a high-intense peak for H17, which confirmed the abundance of complex carbohydrates in the hexane extract of KO. The distinct narrow peak E19 of Figure 1(B) existing at ~723 cm^{-1} represented the rocking vibration of the methylene group, confirming the presence of biomolecules with aliphatic hydrocarbon chains in EtOAc extracts (Coates, 2000; Nandiyanto et al., 2019). Here again, KO displayed a high-intense peak for E19 indicating the higher abundance of aliphatic hydrocarbons in the EtOAc extract of KO. However, this particular mode of vibration was non-existent among MeOH extracts. According to Figure 1(C), peak M18 existing at 903-925 cm^{-1} is usually assigned to C–C stretching vibrations of alkanes in the MeOH extracts (Nandiyanto et al., 2019). Among MeOH extracts, both ST and KK showed only a minute peak for M18 (~903-925 cm^{-1}), which indicated the comparatively lower abundance of C–C stretching vibrations of alkanes. Almost all MeOH extracts exhibited peak M19 at ~630 cm^{-1} which would result due to the alkyne C–H bending vibration of aromatic rings and O–H out-of-plane bending of alcohols (Coates, 2000; Nandiyanto et al., 2019). Both KO and YK showed high-intense peaks for M19.

3.6. α-Glucosidase inhibitory activity

The results of α-glucosidase inhibitory activities (IC_{50} values) of all crude plant extracts are presented in Table 3. Except the MeOH extract of KK, all crude plant extracts exerted some inhibitory activity against α-glucosidase. The higher inhibitory potentials, lower IC_{50} values were exhibited by most of the hexane extracts except KO and LE. Significant ($p < 0.05$) differences were exhibited by all hexane extracts for inhibitory activity (IC_{50} values) against α-

glucosidase enzyme, whereas the highest and the lowest activities were displayed by YK (IC_{50} = 7.71 ± 0.40 ppm) and KK (IC_{50} = 56.51 ± 1.26 ppm), respectively. Among EtOAc extracts, the IC_{50} values followed the order of LE < YK < ST < KK < KO, and no significant (p > 0.05) difference was seen between KK and ST. LE exhibited the strongest inhibitory activity against α-glucosidase with an IC_{50} value of 30.97 ± 0.45 ppm, while the lowest activity was exerted by KO. Among MeOH extracts, IC_{50} values followed the order of KO < LE < YK < ST < KK. KO displayed the strongest inhibitory activity (IC_{50} = 18.08 ± 0.27 ppm), while KK (IC_{50} > 2000 ppm) exhibited the weakest inhibitory activity. Establishing correlations between FTIR spectral data and α-glucosidase inhibitory activities of the plant extracts is in line with the objective of this study as to identify functional groups of the chemical constituents, responsible for α-glucosidase inhibitory activity of plant extracts.

Table 3. IC_{50} values of α-glucosidase inhibitory activities of different crude plant extracts[1]

Leafy plant type	IC_{50} value/ppm		
	Hexane	EtOAc	MeOH
LE	$37.58^{d,B}$ ± 1.05	$30.97^{a,A}$ ± 0.45	$42.7^{b,C}$ ± 2.12
KK	$56.51^{e,A}$ ± 1.26	$151.50^{c,B}$ ± 11.84	ND
KO	$31.72^{c,B}$ ± 0.13	$425.98^{d,C}$ ± 14.13	$18.08^{a,A}$ ± 0.27
ST	$21.79^{b,A}$ ± 0.81	$130.85^{c,B}$ ± 0.32	$225.57^{d,C}$ ± 8.85
YK	$7.71^{a,A}$ ± 0.40	$85.24^{b,B}$ ± 2.27	$125.14^{c,C}$ ± 5.41

[1] Each value in the table represents mean of three replicates ± standard deviation. Means that do not share a similar simple superscription letter in the same column and similar capital superscription letter in the same raw are significantly different at 95% confident (α = 0.05). Abbreviations: LE, *Le-kola pala*; KK, *Kora kaha*; KO, *Koppa*; ST, *Stevia*; YK, *Yaki naran*; ND, Not detected.

Table 4. Summary of PLS regression analysis performed for FTIR spectral data and α-glucosidase inhibitory activities of different crude plant extracts[1]

Model no	Region	Rc^2	RMSEC	Rcv^2	RMSECV	Rp^2	RMSEP
1	A	0.81	50.25	0.60	78.24	0.77	46.40
2	B	0.96	24.10	0.87	41.70	0.93	26.04
3	C	0.71	61.14	0.52	80.21	0.45	71.56
4	D	0.95	24.93	0.87	39.12	0.18	87.79
5	E	0.90	35.14	0.61	73.78	0.79	44.32
6	A, B, C, D, E	0.90	36.72	0.75	56.80	0.73	50.20
7	A, C	0.88	39.53	0.72	60.61	0.85	37.35
8	A, C, E	0.90	35.30	0.84	49.41	0.80	43.25
9	A, D, E	0.91	34.56	0.81	50.12	0.77	46.05
10	A, C, D, E	0.91	34.43	0.77	55.13	0.79	44.32
11	B, D, E	0.91	33.72	0.82	49.97	0.69	53.93
12	D, E	0.92	32.67	0.85	45.19	0.74	49.88
13	C, D, E	0.95	26.38	0.85	44.23	0.84	39.10
14	B, E	0.92	32.78	0.77	56.28	0.87	34.91

[1] A: 3700-2800 cm^{-1}, B: 1800-1700 cm^{-1}, C: 1700-1500 cm^{-1}, D: 1500-900 cm^{-1}, E: 900-500 cm^{-1}. Rc^2: Coefficient of determination of calibration, Rp^2: Coefficient of determination of prediction, Rcv^2: Coefficient of determination of cross validation, RMSEC: Root mean square errors of calibration, RMSEP: Root mean square errors of prediction, RMSECV: Root mean square errors of cross validation

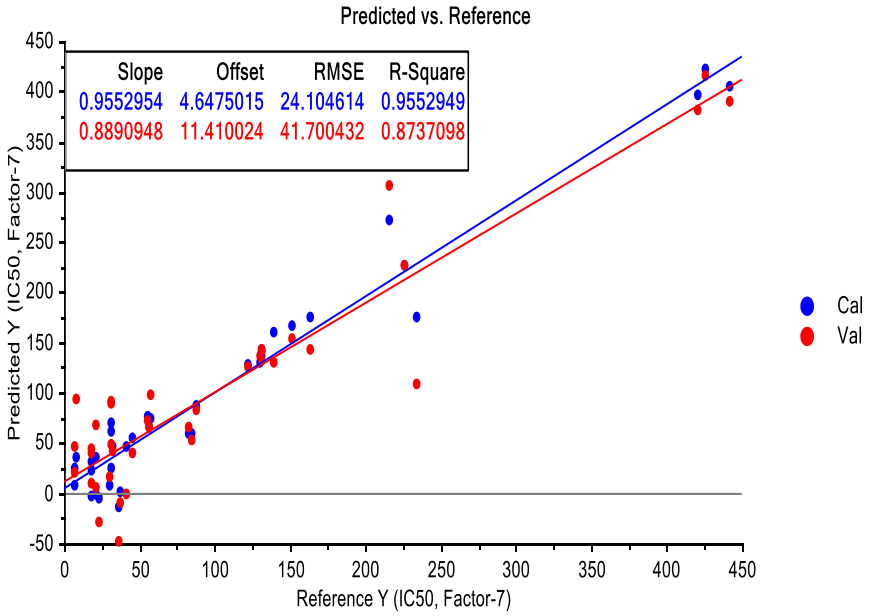

Figure 2. PLS regression (calibration and validation) curves of the best predictive model (Model 2)

3.7. PLS regression analysis

A summary of PLS regression analysis for FTIR spectral data and α-glucosidase inhibitory activities of different crude plant extracts is presented in Table 4. When considering the predictive models developed for individual spectral regions (A, B, C, D, and E), the highest Rc^2 (0.96), Rcv^2 (0.87), Rp^2 (0.93), and the lowest RMSEC (24.10), RMSECV (41.70), and RMSEP (81.04) values were noticed for "Model 2". Meanwhile, "Model 3" was found to show the lowest Rc^2 (0.71), Rcv^2 (0.52), and Rp^2 (0.45), and the highest RMSEC (61.14) and RMSECV (80.21). However, in the case of predictive models developed using selected multiple regions, the highest Rc^2 (0.95), Rcv^2 (0.85), Rp^2 (0.84), and the lowest RMSEC (26.38), and RMSECV (44.23) values were found for "Model 13". The calibration and validation curves for the best PLS regression prediction model "Model 2" are shown in Figure 2. According to PLS regression results, it was evident that the chemical compounds representing spectral region B have had a strong impact on the α-glucosidase inhibitory activity when compared to those of other spectral regions. The spectral region B, ranging from 1700-1800 cm^{-1}, actually represented the presence of chemical constituents with functional groups such as ester linkages, ketone groups, and carboxylic acids as mentioned previously in Tables 1 and 2. Interestingly, compounds with these functional groups which have a higher content of non-polar moieties with ester linkage are mostly present in both hexane and EtOAc extracts.

In these five edible plants, a group of chemical constituents called cinnamic acids, which include sinapic acid, ferulic acid, *p*-coumaric acid, and caffeic acid, are present. They are a common form of phenolic compounds, usually present in plants as esters of sugars and different organic acids (Vermerris & Nicholson, 2008). As described previously, the peak that appeared at ~1740 cm^{-1} would be due to the C=O stretching vibration of ester bonds resulting from these cinnamic acids. According to Pandi and Kalappan (2021), sinapic acid may be present in either the free form or as an ester group; the predominant sinapoyl ester present in leaves is sinapoyl malate. In addition, ferulic acid found in leafy plants can be also conjugated with mono-, di-, and poly-saccharides through ester-linkage (Mancuso & Santangelo, 2014). Ferreira et al. (2019) previously stated that *p*-coumaric acid usually esterifies either with long-chain alkyl alcohols or polysaccharides to produce water-insoluble conjugates of *p*-coumaric acid. In another study Vermerris and Nicholson (2008) found that caffeic acid conjugated with quinic acid through ester linkages to produce chlorogenic acid, which was also previously reported to exist in the five edible leafy plant types (Ulpathakumbura et al., 2023). Vermerris and Nicholson (2008) further mentioned that catechins could also be present in plant extracts in the form of gallic acid esters. Hence, it became evident that the compounds with ester-linkage would have a strong influence on the α-glucosidase inhibitory activity. Further to this, the peak at ~1700 cm^{-1} would results due to the C=O stretching vibration of ketones and carboxylic acids. These carboxylic acids could be hydroxy-benzoic acids present in the leafy plant extracts, which are characterized by the existence of a carboxyl group substituted on a phenol (Vermerris & Nicholson, 2008). The keto groups could also be present in heterocycle flavones such as quercetin, and kaemferol of leafy plants. Hence, it became evident that the compounds with ester-linkage, ketones, and carboxylic acids would have a strong impact on the α-glucosidase inhibitory activity of leafy plant extracts.

4. Conclusions

The FTIR spectral correlations with the anti-hyperglycemic effect of different solvent extracts of selected edible leafy plants of Sri Lanka were explored. All plant extracts exerted inhibitory activity against α-glucosidase except the MeOH extract of KK. Based on PLS regression analysis, a strong correlation was seen between α-glucosidase inhibitory activities of the plant extracts and FTIR spectral data. PLS regression results showed that the chemical constituents represented by the spectral region B (1800-1700 cm^{-1}) of the plants have had a strong relationship with the α-glucosidase inhibitory activity when compared to those of other spectral regions. This particular range (1700-1800 cm^{-1}) is usually ascribed to C=O stretching vibration of ester groups, ketones, or carboxylic acids. This study suggests that FTIR spectroscopic method together with PLS regression analysis can be further explored as an alternative rapid analytical tool for the detection of the anti-hyperglycemic effect of leafy-plant extracts.

Acknowledgments

The expert advice on plant identifcation by Dr. D.S.A. Wijesundera is greatfully acknowledged. The authors also gratefully acknowledge the financial support from National Institute of Fundamental Studies, Sri Lanka for this study.

Conflict of interest

The authors confirm that there are no known conflicts of interest.

Statement of ethics

In this study, no method requiring the permission of the "Ethics Committee" was used.

Availability of data and materials

All data generated or analyzed during this study are included in this published article.

Funding

This study was financially supported by National Institute of Fundamental Studies, Sri Lanka.

CRediT authorship contribution statement

Savani Ulpathakumbura: Formal analysis, Data curation, Methodology, Review & Editing, Writing original draft
Nazrim Marikkar: Conceptualization, Methodology, Project administration, Review & Editing, Writing-reviewing & Editing
Lalith Jayasinghe: Writing-reviewing & Editing

ORCID Numbers of the Authors

S. Ulpathakumbura: 0000-0001-8079-0118
N. Marikkar: 0000-0002-6926-2071
L. Jayasinghe: 0000-0003-1703-4154

Supplementary File

None.

Publisher's Note

All claims expressed in this article are solely those of the authors and do not necessarily represent those of their affiliated organizations, or those of the publisher, the editors and the reviewers. Any product that may be evaluated in this article, or claim that may be made by its manufacturer, is not guaranteed or endorsed by the publisher.

References

Adina, C., Florinela, F., Abdelmoumen, T., & Carmen, S. (2010). Application of FTIR spectroscopy for a rapid determination of some hydrolytic enzymes activity on sea buckthorn substrate. *Romanian Biotechnological Letters, 15*(6), 5738-5744.

Ashokkumar, R., & Ramaswamy, M. (2014). Phytochemical screening by FTIR spectroscopic analysis of leaf extracts of selected Indian medicinal plants. *International Journal of Current Microbiology and Applied Sciences, 3*(1), 395-406.

Bhardwaj, M., Yadav, P., Dalal, S., & Kataria, S. K. (2020). A review on ameliorative green nanotechnological approaches in diabetes management. *Biomedicine & Pharmacotherapy, 127*, 110198.

Bunaciu, A. A., Aboul-Enein, H. Y., & Fleschin, S. (2011). Recent applications of fourier transform infrared spectrophotometry in herbal medicine analysis. *Applied Spectroscopy Reviews, 46*(4), 251-260.

Coates, J. (2000). Interpretation of infrared spectra, a practical approach. In R. A. Meyers (Ed.), *Encyclopedia of Analytical Chemistry*: US: John Wiley & Sons, Ltd.

De Souza Schmidt Goncalves, A. E., Lajolo, F. M., & Genovese, M. I. (2010). Chemical composition and antioxidant/antidiabetic potential of Brazilian native fruits and commercial frozen pulps. *Journal of Agricultural and Food Chemistry, 58*(8), 4666-4674.

Easmin, S., Sarker, M. Z. I., Ghafoor, K., Ferdosh, S., Jaffri, J., Ali, M. E., Mirhosseini, H., Al-Juhaimi, F. Y., Perumal, V., *et al.* (2017). Rapid investigation of α-glucosidase inhibitory activity of *Phaleria macrocarpa* extracts using FTIR-ATR based fingerprinting. *Journal of Food and Drug Analysis, 25*(2), 306-315.

Ediriweera, E., & Ratnasooriya, W. (2009). A review on herbs used in treatment of diabetes mellitus by Sri Lankan ayurvedic and traditional physicians. *Ayu, 30*(4), 373-391.

Ferreira, P. S., Victorelli, F. D., Fonseca-Santos, B., & Chorilli, M. (2019). A review of analytical methods for *p*-coumaric acid in plant-based products, beverages, and biological matrices. *Critical Reviews in Analytical Chemistry, 49*(1), 21-31.

Gunarathne, R., Marikkar, N., Mendis, E., Yalegama, C., Jayasinghe, L., Liyanage, R., & Jayaweera, S. (2022a). Bioactivity studies of different solvent extracts of partially defatted coconut testa obtained from selected coconut cultivars. *The Journal of Agricultural Sciences-Sri Lanka, 17*(1), 171-184.

Gunarathne, R., Marikkar, N., Mendis, E., Yalegama, C., Jayasinghe, L., & Ulpathakumbura, S. (2022b). Mid-IR Spectral Characterization and Chemometric Evaluation of Different Solvent Extracts of Coconut Testa Flour. *Journal of Food Chemistry and Nanotechnology, 8*(3), 69-75.

Gunarathne, R., Marikkar, N., Yalegama, C., & Mendis, E. (2022c). FTIR spectral analysis combined with chemometrics in evaluation of composite mixtures of coconut testa flour and wheat flour. *Journal of Food Measurement and Characterization, 16*(3), 1796-1806.

Hari, N., & Nair, V. P. (2018). FTIR spectroscopic analysis of leaf extract in hexane in *Jasminum azoricum* L. *Recent Research in Science and Technology, 4*(8), 170-172.

Jayaraj, S., Suresh, S., & Kadeppagari, R. K. (2013). Amylase inhibitors and their biomedical applications. *Starch-Stärke, 65*(7-8), 535-542.

Kazeem, M., Adamson, J., & Ogunwande, I. (2013). Modes of inhibition of α-amylase and α-glucosidase by aqueous extract of *Morinda lucida* Benth leaf. *BioMed Research International, 2013*, 527570.

Mancuso, C., & Santangelo, R. (2014). Ferulic acid: Pharmacological and toxicological aspects. *Food and Chemical Toxicology, 65*, 185-195.

Mittal, P., Goswami, M., & Airi, M. (2020). Phytochemical, FTIR and NMR Analysis of Crude Extract of *Duranta plumieri* leaves. *Journal of Pharmaceutical Sciences and Research, 12*(1), 182-185.

Nandiyanto, A. B. D., Oktiani, R., & Ragadhita, R. (2019). How to read and interpret FTIR spectroscope of organic material. *Indonesian Journal of Science and Technology, 4*(1), 97-118.

Nickavar, B., & Abolhasani, L. (2013). Bioactivity-guided separation of an α-amylase inhibitor flavonoid from *Salvia virgata*. *Iranian Journal of Pharmaceutical Research, 12*(1), 57-61.

Nipun, T. S., Khatib, A., Ahmed, Q. U., Redzwan, I. E., Ibrahim, Z., Khan, A. a. Y. F., Primaharinastiti, R., Khalifa, S. A., & El-Seedi, H. R. (2020). Alpha-glucosidase inhibitory effect of *Psychotria malayana* jack leaf: A rapid analysis using infrared fingerprinting. *Molecules, 25*(18), 4161.

Nokhala, A., Ahmed, Q. U., Saleh, M. S., Nipun, T. S., Khan, A. A. Y. F., & Siddiqui, M. J. (2020). Characterization of α-glucosidase inhibitory activity of *Tetracera scandens* leaves by fourier transform infrared spectroscopy-based metabolomics. *Advances in Traditional Medicine, 20*, 169-180.

Pandi, A., & Kalappan, V. M. (2021). Pharmacological and therapeutic applications of Sinapic acid—An updated review. *Molecular Biology Reports, 48*(4), 3733-3745.

Saleh, M. S., Siddiqui, M. J., Mat So'ad, S. Z., Roheem, F. O., Saidi-Besbes, S., & Khatib, A. (2018). Correlation of FT-IR fingerprint and α-glucosidase inhibitory activity of salak (*Salacca zalacca*) fruit extracts utilizing orthogonal partial least square. *Molecules, 23*(6), 1434.

Shobana, S., Sreerama, Y., & Malleshi, N. (2009). Composition and enzyme inhibitory properties of finger millet (*Eleusine coracana* L.) seed coat phenolics: Mode of inhibition of α-glucosidase and pancreatic amylase. *Food Chemistry, 115*(4), 1268-1273.

Ulpathakumbura, S., Marikkar, N., & Jayasinghe, L. (2023). Anti-oxidative, anti-hyperglycemic and anti-obesity properties of selected edible leafy plants of Sri Lanka. *Food Chemistry Advances, 2*, 100208.

Umar, A. H., Ratnadewi, D., Rafi, M., & Sulistyaningsih, Y. C. (2021). Untargeted metabolomics analysis using FTIR and UHPLC-Q-Orbitrap HRMS of two *Curculigo* species and evaluation of their antioxidant and α-glucosidase inhibitory activities. *Metabolites, 11*(1), 42.

Vermerris, W., & Nicholson, R. (2008). Families of Phenolic Compounds and Means of Classification. In W. Vermerris & R. Nicholson (Eds.), *Phenolic Compound Biochemistry* (pp. 1-34): Springer, Dordrecht.

White, J. L. (1971). Interpretation of infrared spectra of soil minerals. *Soil Science, 112*(1), 22-31.

Xiao-Ping, Y., Chun-Qing, S., Ping, Y., & Ren-Gang, M. (2010). α-Glucosidase and α-amylase inhibitory activity of common constituents from traditional Chinese medicine used for diabetes mellitus. *Chinese Journal of Natural Medicines, 8*(5), 349-352.